International Journal of Pharmaceutics 606 (2021) 120885

Contents lists available at ScienceDirect

International Journal of Pharmaceutics

journal homepage: www.elsevier.com/locate/ijpharm

Novel tip-loaded dissolving and implantable microneedle array patches for sustained release of finasteride

Alejandro J. Paredes [a], Fabiana Volpe-Zanutto [a], Andi Dian Permana [b], Aidan J. Murphy [a], Camila J. Picco [a], Lalitkumar K. Vora [a], Jonathan A. Coulter [a], Ryan F. Donnelly [a,*]

[a] School of Pharmacy, Queen's University Belfast, 97 Lisburn Road, Belfast BT9 7BL, UK
[b] Department of Pharmaceutics, Faculty of Pharmacy, Hasanuddin University, Makassar, Indonesia

ARTICLE INFO

Keywords:
Microarray Patches
Long-acting
Finasteride
Microneedles
PLGA

ABSTRACT

Finasteride (FND) is a competitive inhibitor of 5α-reductase, an enzyme involved in benign prostatic hyperplasia (BPH) and androgenic alopecia. FND is administered in oral, often lifelong treatments, increasing the pill burden of polymedicated patients. Microneedle array patches (MAPs) are minimally invasive devices that painlessly pierce the outermost layers of the skin, forming slowly-dissolving drug depots in the dermis, which can release drugs over weeks or months, making this platform an attractive, patient-friendly option for long-term treatments. This work describes the development of long-acting dissolving and implantable PLGA MAPs aimed for systemic release of FND for at least two weeks. Mechanically strong tip-loaded MAPs with pyramidal geometry were obtained using micromoulding methodology. *In vitro* studies revealed that the dissolving and implantable MAPs were able to release the drug for over 7 and 14 days, respectively. Skin deposition experiments in Franz cells demonstrated that after 24 h, dissolving and implantable MAPs were able to deposit 629.00 ± 214.54 μg and 1861.64 ± 383.30 μg of FND in the skin, respectively. On the other hand, transdermal permeation studies showed that both formulations produced a slow release of the drug to the receptor compartment of the Franz cells, with dissolving and implantable MAPs releasing 90.43 ± 6.20 μg and 27.80 ± 3.94 μg of FND after 24 h. The formulations described here could be an alternative to current oral treatments, having the potential to deliver the drug for extended periods, simplifying the treatment of BPH and androgenic alopecia.

1. Introduction

Finasteride (FND) is a competitive inhibitor of 5α-reductase, an enzyme that causes a decrease in serum dihydrotestosterone concentrations, a hormone heavily involved in benign prostatic hyperplasia (BPH) and androgenic alopecia (Gormley et al., 1992). FND is currently approved at an oral dose of 1 mg/day for the treatment of androgenic alopecia and 5 mg/day for the relief of symptoms as well as progression prevention of BPH (D'Amico and Roehrborn, 2007; Gormley et al., 1992). Moreover, long-term clinical studies have shown that FND has a preventive effect on the development of prostate cancer (Goodman et al., 2019; Thompson et al., 2003). FND is prescribed in long-term, often lifelong treatments, contributing to the increase of the pill burden of patients with chronic diseases (Chiu et al., 2009; Claborn et al., 2015). Furthermore, only 63% of the drug is absorbed in the gastrointestinal tract (Steiner, 1996), and patients under oral treatment with FND might present side effects such as depression, loss of libido, and erectile dysfunction (NHS, 2020). Consequently, and aiming to optimize the delivery of the drug, several topical formulations have been developed based on chemical enhancers (Rao et al., 2008), liposomes (Kumar et al., 2007; Tabbakhian et al., 2006), polymeric nanoparticles (Ahmed, 2016; Pervaiz et al., 2020; Roque et al., 2017), PLGA microspheres (Kim et al., 2019) and microemulsions (Soleymani and Salimi, 2019). However, these approaches have shown limited success due of their low drug loading capacity and the need for continuous and long-term application on the skin, which also reflects in the fact that none of these formulations have reached the market. In this context, the development of novel formulations that can be administered in an easy, non-invasive manner to the skin, delivering the active agent systemically for weeks after a single application is an interesting proposition.

Microneedle array patches (MAPs) consist of a baseplate from which multiple and regularly interspaced micro-projections (microneedles,

* Corresponding author at: Chair in Pharmaceutical Technology School of Pharmacy Queen's University Belfast Medical Biology Centre, 97 Lisburn Road, Belfast BT9 7BL, UK.
E-mail address: r.donnelly@qub.ac.uk (R.F. Donnelly).

https://doi.org/10.1016/j.ijpharm.2021.120885
Received 1 June 2021; Received in revised form 8 July 2021; Accepted 10 July 2021
Available online 14 July 2021

MNs) protrude (Paredes et al., 2020b). These MNs are able to pierce the *stratum corneum*, localising their drug cargo in the viable layers of the skin, from where the active agent can diffuse into the skin microcirculation, facilitating systemic distribution (Paredes et al., 2020b; Permana et al., 2020). Moreover, MAPs can be self-applied without causing pain or drawing blood, making this platform an attractive alternative to injectable treatments (Donnelly and Larrañeta, 2018). Even though MAPs were initially designed for the administration of vaccines and small molecules with low doses and high potency, the delivery of a wider variety of drugs continues to gain momentum (Paredes et al., 2020b; Yang et al., 2019). Crucially, MAPs have the ability to deliver medications for weeks or months after short wearing periods, potentially leading to enhanced treatment adherence and patient compliance, which constitutes a significant advantage in comparison to oral formulations that require daily administration (Chen et al., 2020; Vora et al., 2021). In particular, dissolving/bioresorbable MAPs are among the most promising strategies for long-acting release since they are made of polymers that dissolve or slowly degrade in the skin, exposing a drug depot to subsequent gradual dissolution in the fluids of the dermis (Paredes et al., 2021). The release of the drug from a MAP will largely depend on the physicochemical properties of active substance, although it can be modulated by varying the concentration and the nature of the polymers used to fabricate the MNs (Larrañeta et al., 2016; Van Der Maaden et al., 2012). A large variety of natural and synthetic polymers have been used to manufacture MAPs, such as polyvinyl alcohol (PVA), polyvinyl pyrrolidone (PVP), polylactic acid (PLA), poly(lactic-co-glycolic) acid (PLGA), Gantrez® and hyaluronic acid, among others (Larrañeta et al., 2016; Lee et al., 2008). A previous report describing a powder-carrying microneedle-based formulation for local delivery of FND, demonstrated the potential of the system to promote hair growth in mice (S. Kim et al., 2019). However, these patches must be applied in large areas of the scalp every three days, with hair growth possibly impeding correct MN insertion.

In this work, we describe for the first time the formulation of dissolving PVP/PVA, and implantable PLGA MAPs that could be applied in the arm, for instance, and release the drug systemically for at least two weeks (Fig. 1). The systems were characterised both in terms of their physiochemical and mechanical properties. The insertion of the MNs was evaluated using optical coherence tomography (OCT) and *in vitro* drug release assayed using dialysis membranes. Finally, Franz cells were used to analyse the skin deposition and transdermal drug delivery in excised full-thickness neonatal porcine skin.

2. Materials and methods

2.1. Materials

Finasteride of > 99.5% purity was obtained from Beijing Bocai Pharma Tech (Suzhou, China). Polyvinylpyrrolidone (PVP K29-32; and K90) was purchased from Ashland (Kidderminster, UK). Poly(vinyl alcohol) (PVA 9–10 kDa), Poloxamer 188 (Kolliphor® P188), trifluoroacetic acid (TFA), acetonitrile (ACN), methanol (MeOH) and dimethyl sulfoxide (DMSO) were purchased from Sigma-Aldrich (Dorset, UK). Poly(D,L-lactide-co-glycolide) (PLGA) with a lactide:glycolide ratio of 75:25 and ester end, Viatel® DLG 7503 E, was kindly gifted by Ashland (Kidderminster, UK). Phosphate buffered saline (PBS) tablets were obtained from Oxoid Ltd, Thermo Fischer Scientific, Massachusetts, USA. In all cases, Elga purified water was used (Purelab option, Elga LabWater, High Wycombe, UK). All other chemicals used in this work were of analytical grade.

2.2. Manufacture of dissolving and implantable MAPs

Tip loaded FND MAPs were prepared using silicone moulds with

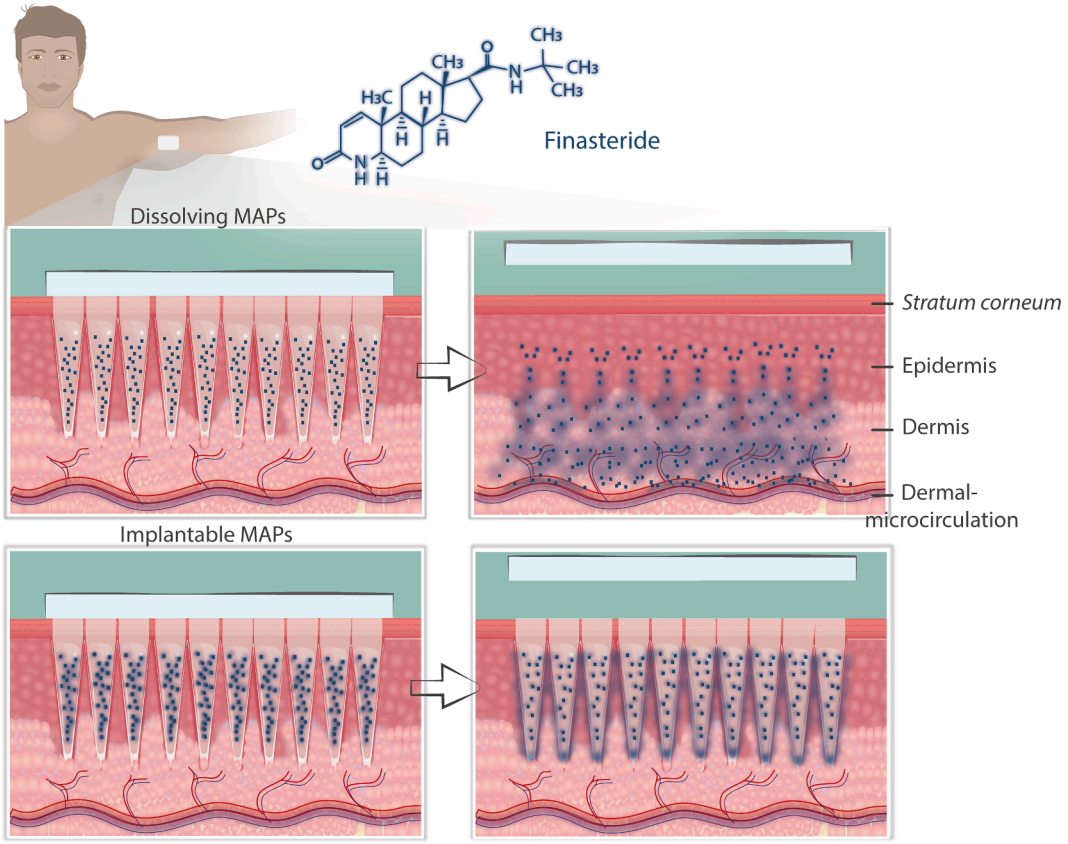

Fig. 1. Chemical structure of finasteride and description of the proposed long-acting release MAPs.

pyramidal needles of 850 μm height (600 μm pyramidal tip, 250 μm base column), a needle density of 16 × 16 (in 0.5 cm^2), 300 μm width at the base and 300 μm interspacing. A mixture of PVP and PVA was used to make a suspension with FND incorporated. The first layer (MNs layer) of the dissolving MAPs was prepared by mixing 0.84 g of FND, 1.2 g of a blend containing 40% w/w PVP and PVA at a mass ratio 1:1, and 1 ml of water in a DAC 150 FVZ SpeedMixer™ (High Wycombe, England) at a 3775 g for 10 min. The first layer of the implantable MAPs was prepared by dissolving 0.3 g of PLGA in 0.5 ml of DMSO and adding 0.2 g of FND. The sample was homogenised using the SpeedMixer™ at 5000 rpm for 6 min. Dissolving and implantable blends were separately poured in excess on top of the silicone moulds and placed in a pressure chamber for 2.5 min at 5 bar to facilitate the filling of MN cavities. Afterward, the first layer excess was carefully removed using a spatula, and a holder ring was attached to the silicone moulds using PVA 40% w/w as glue. The baseplate, composed of 850 μl of PVP K90 30% w/w in water, was added into the ring holder and centrifuged at 3,500 rpm for 15 min. The MAPs were left to dry for 1.5 days at ambient conditions, separated from the ring and excess polymer at the baseplate edge removed using scissors. The fabrication process is illustrated in Fig. 2**a**. MAPs were examined visually using a Leica EZ4W stereomicroscope (Leica Microsystems, Milton Keynes, UK) and a VHX digital microscope (Keyence, Ltd, Milton Keynes, UK).

2.3. Physical testing and insertion of MAPs

Mechanical strength and insertion studies were carried out on the MAPs using a TA.XT2 Texture Analyser (Stable Micro Systems., Ltd., Haslemere, UK) as illustrated in Fig. 2b. The apparatus was set in compression mode, applying a force of 32 N for 30 s vertically at a downward speed of 1.19 mm/s, representing the average human force applied during MAPs application as shown in past studies (Larrañeta et al., 2014). MNs height reduction was tested using the same experimental setup, vertically compressing the MAPs against a solid flat aluminium surface, where the height of the MNs were measured before and after compression using a microscope. The experiments were carried out in six MAPs (n = 6) and the results expressed in terms of percentage height reduction. Insertion studies were carried out using Parafilm M® (Bemis Company Inc., Soigneis, Belgium) as a skin simulant model, cut to form eight layers that were stacked one on top of the other. This method has previously shown good correlation with results obtained from skin studies (Larrañeta et al., 2014). Insertion studies were performed using six MAPs (n = 6), with insertion quantified by counting the number of perforations in each layer when separated. Individual layers were examined under a Leica EZ4W stereomicroscope using two polarizer filters.

2.4. Determination of FND in whole MAPs, MN tips and baseplates

Drug content analysis was carried out to determine the amount of FND in whole MAPs, and the drug distribution between the MN tips and the baseplates. For whole MAPs, each patch was placed in 5 ml of deionised water and magnetically stirred for 15 min, 5 ml of methanol were added, and further agitation applied for 15 min. Afterward, a 100 μl aliquot was taken and diluted with 900 μl of acetonitrile in order to precipitate the hydrophilic polymers PVP and PVA. To assess the drug distribution between MN tips and baseplates, the MN tips were carefully separated from the baseplates using a scalpel and collected in a 12 ml glass vial. The baseplates and MN tips of each patch were treated with the same extraction protocol used for entire MAPs, with the exception of the implantable MN tips, which were also sonicated for 30 min at room temperature to ensure total extraction of the drug. Centrifugation at 14,000 rpm for 15 min was applied in all samples before drug quantification using the method described in section 2.5. Whole MAPs, MN tips and baseplates of dissolving and implantable MAPs were analysed by triplicate.

2.5. HPLC analysis of FND

Analysis of FND was carried out using a reverse-phase high-performance liquid chromatography (RP-HPLC). Analysis was performed on an Agilent 1220 Infinity LC System (Agilent Technologies UK Ltd.,

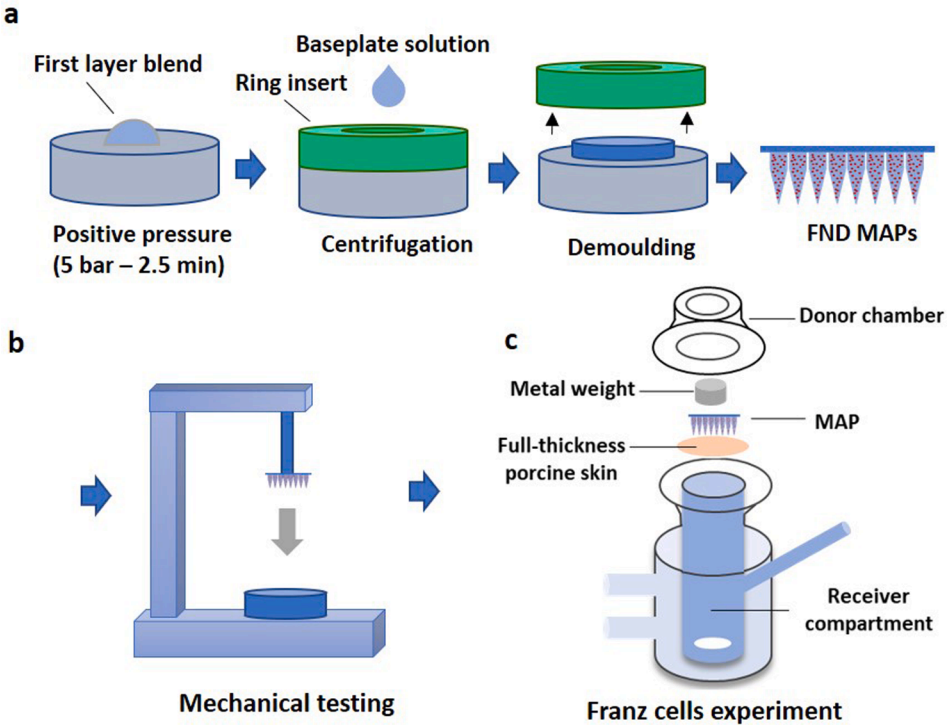

Fig. 2. Manufacture and characterisation of dissolving and implantable FND MAPs. a- casting method used to prepare the dissolving and implantable MAPs. b- mechanical characterisation of MAPs using a texturometer. c- Skin studies in using Franz cells.

Stockport, UK) with a Zorbax Eclipse® XDB-C18 column (4.6 × 50 mm, 1.8 μm; Agilent Technologies, Santa Clara, United States) and UV detection at 210 nm. The column temperature was maintained at 25℃. Following a number of iterations, suitable chromatographic separation was achieved using a mobile phase consisting of 60% ACN and 40% TFA 0.1% v/v at flow rate was 0.5 ml/min and an injection volume of 25 μl. Calibration curves were obtained in a concentration range of 0.1 to 100 μg/ml with a correlation level (r^2) of 1. The limit of detection (LoD) was 0.95 μg/ml and limit of quantification (LoQ) was 2.89 μg/ml. The method was highly selective for FND when it was extracted from MAPs and skin. The full linearity, accuracy and precision data can be found in **Figure S1** and **Tables S1-3** in the supplementary material.

2.6. Fourier transform infrared spectroscopy (FTIR)

Scans were performed using an FTIR (Fourier Transform Infrared Spectroscopy) Accutrac FT/IR-4100 Series (Jasco, Essex, UK) equipped with Diamond MIRacle™ ATR, in the region of 4000–600 cm^{-1} at a resolution of 4.0 cm^{-1}. An average of 64 repeat scans was taken to obtain each spectrum.

2.7. Thermal analysis

Change in state of the dissolving MAPs was investigated by differential scanning calorimetry (DSC). DSC studies were carried out with a TA Instruments DSC Q100 (TA Instruments, New Castle, Delaware, USA). The temperature range was 25 to 280℃ with a heating speed of 10℃/min and nitrogen flow rate of 10 ml/min. Thermogravimetric analysis (TGA) was carried out using a Q500 thermogravimetric analyser. The heating rate was calibrated at 10℃/min in the range of 25℃ to 500℃. The data from the DSC and thermogravimetric analysis experiments were analysed with TA Instruments Universal Analysis, version 4.5A.

2.8. Powder X-ray diffraction (PXRD)

The crystalline characteristics of FND alone and included in dissolving and implantable MAPs was assessed using a Miniflex™ X-ray powder diffractometer (Rigaku Corporation, Tokyo, Japan) equipped with Ni-filtered, Cu Kβ radiation, at a current of 15 mA and a voltage of 30 kV as described in a previous work (Volpe-Zanutto et al., 2021).

2.9. Particle size analysis

The particle size of coarse FND and FND dispersed from dissolving MAPs was determined by laser diffraction using a Mastersizer® 3000 equipped with a Hydro® cell (Malvern Panalytical Ltd, Worcestershire, England). To this purpose, 20 mg of the coarse drug were dispersed with a vortex in 10 ml of 2% w/v of Poloxamer 188 to ensure particle disaggregation. For the dissolving MN tips, the MNs of six dissolving MAPs were scrapped with a scalpel and dispersed in 5 ml of deionised water. For measurement, both samples were dispersed in 500 ml of water, setting the agitation of the Hydro® cell at 2,000 rpms for 3 min, followed by 30 s of sonication. Then the samples were measured six times. The results were expressed in terms of the De Brouckere and Sauter mean diameters ([D4,3] and [D3,2], respectively), and D_{10}, D_{50} and D_{90}.

2.10. In vitro release studies

In vitro release profiles were obtained for pure FND, dissolving MAPs and implantable MAPs using a dialysis membrane method (Mir et al., 2019; Permana et al., 2020). The samples used in this experiment were FND (5 mg), the MNs carefully scraped from three dissolving MAPs, and three implantable MAPs. Each sample was separately dispersed in 1 ml of PBS and placed into Spectra-Por®, 12,000–14,000 MWCO dialysis membrane bags (Spectrum Medical Industries, Los Angeles, CA, USA) and sealed with plastic clamps. The release study was performed in 50 ml of 20% v/v of ethanol in water to ensure sink conditions, using hermetically sealed bottles which were placed at 37C in an orbital incubator (Jeio Tech ISF 7100 Incubator, Ma, USA) at 100 rpm. Aliquots of 1 ml were taken at predetermined time intervals and replaced with an equal volume of fresh release medium. Samples were filtered and quantified by the HPLC methodology described in Section 2.5. Each release experiment was performed in triplicate (n = 3).

2.11. Skin deposition studies

The skin deposition of the FND MAPs were evaluated using excised full-thickness neonatal porcine obtained from stillborn piglets and immediately frozen after birth at −20 °C and defrosted overnight before use. To this purpose, a Franz cells apparatus was set up as shown in Fig. 2**c**. The porcine skin is a widely accepted model for human skin (Summerfield et al., 2015) and has been extensively used for MAPs characterisation in Franz cells (Courtenay et al., 2020; Mc Crudden et al., 2018; Permana et al., 2020). Each skin sample was carefully shaved before use and attached to the donor chamber of each Franz with the *stratum corneum* facing upwards, adhered using cyanoacrylate glue. The donor compartments (with diffusion area of 1.7 cm^2) were placed on a sheet of dental wax covered in aluminium foil and MAPs were manually inserted into the skin. A 10 g stainless steel cylinder of 1.2 cm in diameter and 1 cm in height was placed on top of the MAPs to keep them in place and the donor system mounted onto the receiver compartments, which contained 12 ml of 20% v/v of ethanol in water. The system was maintained at 37 ± 1^{0}C and stirred with a magnetic bar at 600 rpm during the experiment. The joint between the compartments was wrapped in Parafilm® to avoid solvent evaporation. After 24 h, the system was disassembled and the skin area where MAPs were applied was removed using a 1 cm^2 biopsy punch. The drug was extracted by placing the skin pieces in the Eppendorf tubes with 2 ml of MeOH:water (1:1) and two stainless steel beads with a diameter of 0.5 cm (Qiagen, Hilden, Germany) and homogenising them at 50 Hz for 15 min in a Qiagen TissueLyser® LT (UK Quiagen Ltd, Manchester, UK). After centrifugation at 14,000 rpm for 15 min, the supernatants were suitably diluted and analysed by HPLC, together with aliquots obtained from the receptor compartments after the experimental end point. Each Franz cell experiment was carried out in quadruplicate (n = 4).

2.11.1. Transdermal drug delivery

The same experimental set up described in section 2.11 was used to evaluate the transdermal drug permeation using dissolving and implantable MAPs. For this purpose, samples were taken at predetermined time intervals from the receiver compartment until 24 h, centrifuged at 14,000 rpm, suitable diluted and quantified by HPLC. Each experiment was done in 4 replicates (n = 4).

2.12. Optical coherence tomography

MAP insertion into Parafilm M® and skin was visualised by optical coherence tomography (OCT) using a EX1301 OCT Microscope (Michelson Diagnostics Ltd., Kent., UK). Real-time high-resolution imaging of the Parafilm M® layers and skin was enabled by OCT imaging with a laser centre wavelength of 1305.0 ± 15.0 mm. Layers were scanned at a frame rate of 15B-scans (2D cross-sectional scans) per second with a scan width of 2.0 mm. The 2D images were examined using the imaging software ImageJ® (National Institute of Health, Bethesda, USA). Accurate visualization was allowed as the scale of image files was 1.0 pixel = 4.2 μm (Donnelly et al., 2010).

2.13. Statistical analysis

Statistical analysis was carried out using GraphPad Prism© version

8.0 (GraphPad Software Inc, San Diego, California, USA). Data was analysed where appropriate using a one-way analysis of variance (ANOVA). In all cases, $p < 0.05$ denoted significance. Results were expressed as means ± standard deviation (SD).

3. Results and discussion

3.1. MAPs manufacture

Bi-layered dissolving and implantable MAPs were obtained by casting the drug containing layer and the baseplate sequentially. Dissolving MAPs were prepared using PVA and PVA as the basis of a dissolvable matrix, whereas the implantable MAPs contained a first layer made of the biodegradable polymer PLGA. Microscopic analysis revealed all the MNs were correctly formed, with transparent, flat baseplates and MN geometry consisting of a square pedestal with pyramidal tips (Fig. 3). Dissolving MAPs were obtained using a combination of low molecular weight PVP and PVA, two polymers that are able to form mechanically strong MNs, while keeping a rapid dissolution rate in the fluids of the skin, thus exposing the drug particles to dissolution. The dissolvable patches showed clear and uniform separation between the drug-containing layer and the baseplate as observed in Fig. 3**a-c**. On the other hand, implantable MAPs showed a mottled appearance which was related to the solidification of the drug and PLGA after the evaporation of the DMSO used to prepare the first layer solution (Fig. 3**d-f**). The method reported here included the use of a ring insert which allows centrifugation of the mould while keeping the baseplate polymer blend on top of the already formed MNs, facilitating the preparation of bi-layered MAPs. This method is able to produce formulations with the drug concentrated in the first layer and avoids the presence of air bubbles trapped in the viscous baseplate solutions while ensuring good adhesion between the two layers.

3.2. Mechanical characterisation

The mechanical resistance of MNs is critical to efficiently pierce the *stratum corneum* and deposit their drug cargo in the dermis. As observed in Fig. 4, dissolving MAPs presented a MN height reduction of 7.12 ± 2.62% after the application of 32 N compression force against a flat solid aluminium surface, whereas implantable PLGA MAPs showed a reduction of 26.93 ± 0.41%. In the figures obtained by optical microscopy (Fig. 4**a-b**), it can be observed that the MN tips before the test had a pyramidal sharp shape while, after compression, the MNs tips were compacted and showed different levels of reduction in their height. Blends of PVP and PVA have been previously described as efficient MN formers, leading to mechanically resistant formulations (Abdelghany

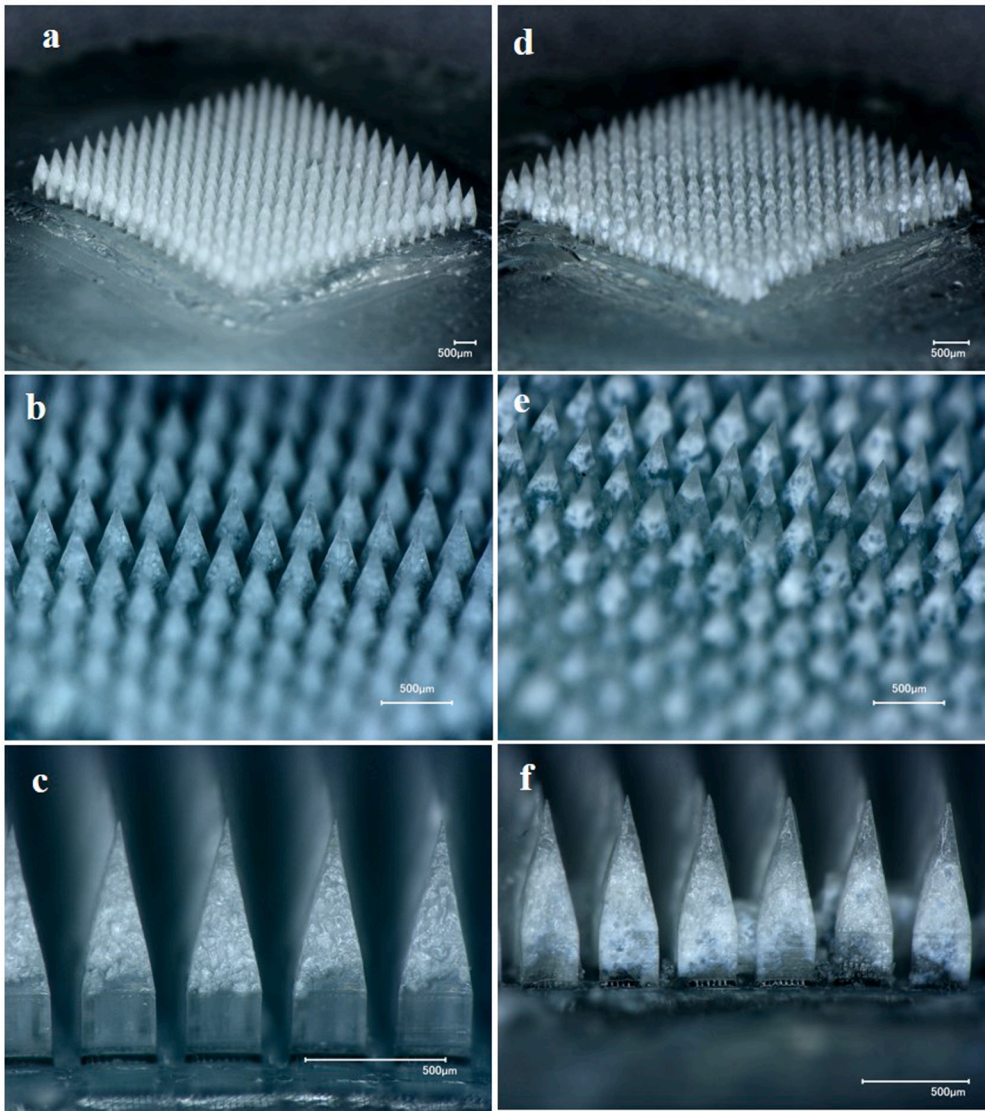

Fig. 3. Optical microscopy images obtained at different magnifications for dissolving MAPs (a-c) and implantable.

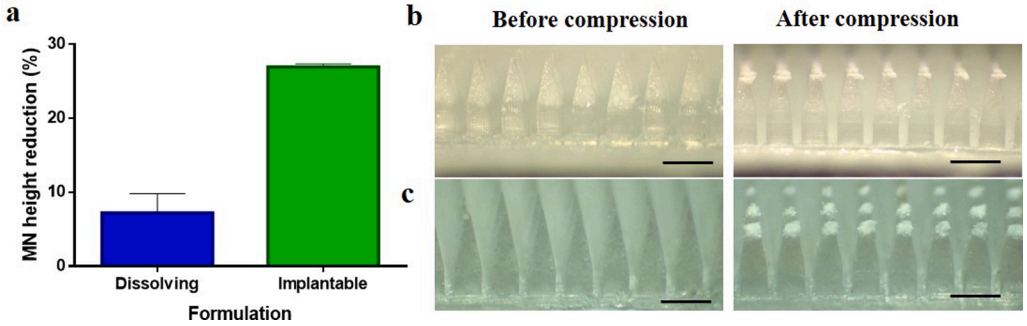

Fig. 4. MNs height reduction for dissolving and implantable MAPs, results expressed as means ± SD, n = 6 (a) and pictures obtained before and after compression of dissolving MAPs (b) and implantable MAPs (c). Scale bar in the microscopy images = 500 μm.MAPs (d-f). Scale bar = 500 μm.

et al., 2019; Permana et al., 2021, 2020) and this has been explained by the interactions between the hydroxyl groups of PVA and the carboxyl groups of PVP (Permana et al., 2019a). In the case of the formulations produced using PLGA, the mechanical resistance was clearly reduced and a waxy consistency was observed during the compression experiments. Other works have reported the use of PLGA for the manufacture of MAPs with demonstrated capability of piercing the skin (He et al., 2020; Li et al., 2019a, 2019b). However, insertion studies were required to fully understand the capability of FND dissolving and implantable MAPs to pierce the skin.

The skin simulant Parafilm® model has been widely used to test the insertion capacity of MAPs (Larrañeta et al., 2014; Permana et al., 2020, 2019b; Volpe-Zanutto et al., 2021). Here, the number of perforations in eight Parafilm® layers that are placed on top of each other is counted after MAP insertion. To date, there are no available standardised tests for the quality control of MAPs; however, previous reports have demonstrated that MN height reductions below 10% and penetration of at least two Parafilm® layers (330 μm in depth) can lead to an efficient skin insertion and drug deposition *in vitro* and *in vivo* (Permana et al., 2020; Tekko et al., 2020; Volpe-Zanutto et al., 2021). As shown in Fig. 5**a**, the first and second Parafilm® layers were pierced by nearly 100% of the MNs for both formulations, whereas a noticeable difference was observed in the number of holes created in the third layer. While dissolving MAPs pierced the third layer with 69.73 ± 4.70% of the MNs, implantable MAPs did it with only 20.51 ± 10.22% of the MNs. This study complements the MNs height reduction assay in order to ensure efficient MN insertion in the skin and successful delivery of the drug. In this study, implantable MAPs showed a greater height reduction but retained good insertion capacity, therefore and aiming to fully understand the ability of implantable MAPs to deliver drugs to the skin, further experiments were carried out as described in the following sections.

3.3. Physicochemical characterisation

Thermal characteristics of FND alone, and FND loaded into dissolving and implantable MN tips, together with their correspondent excipients were investigated using DSC, as depicted in Fig. 6**a and b**, respectively. The DSC thermogram of pure FND exhibited a sharp peak at 258 °C, corresponding to the melting point of the drug and indicating a high degree of crystallinity. The small peak observed in the magnification boxes of Fig. 6a and b is typically present in the DSC profile of polymorph I of FND (da Silva et al., 2015). FND contains an enantiotropic pair (forms I and II), with form I being preferred due to its increased stability and dissolution rate (da Silva et al., 2015; Wawrzycka et al., 1999). Importantly, this characteristic profile was also observed in the thermograms of the dissolving and implantable PLGA MN tips. In the case of the dissolving formulation, the main melting peak appears in a narrow window of temperatures, indicating that the active compound retained a high degree of crystallinity in these MAPs. The implantable MN tips, on the other hand, produced a less defined melting peak for FND and a shift to lower temperatures, which could be attributed to a partial amorphization of FND occurred during drug solidification within the PLGA matrix, or a thermally-induced amorphization of the system during DSC experiments as previously described in the literature (Paredes et al., 2020a; Simonazzi et al., 2018). Further X-ray diffraction experiments detailed below in this section were crucial to unveil the crystalline state of FND in both MAPs. Thermogravimetric (TGA)

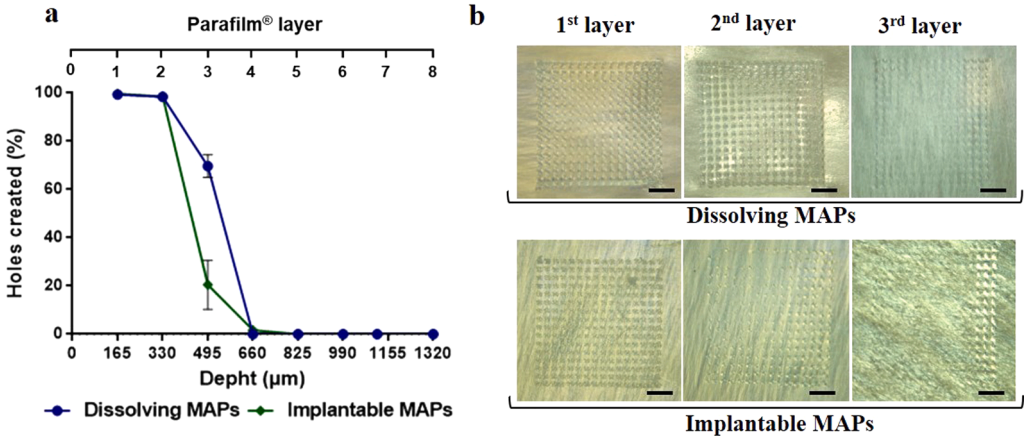

Fig. 5. Insertion test in the Parafilm® skin simulant model. a- percentage of needles piercing each of the eight Parafilm® layers by dissolving and implantable MAPs, results expressed as means ± SD, n = 6. b- optical microscopy images of the first, second and third Parafilm® layers for dissolving and implantable MAPs. Scale bar in the microscopy images = 1 mm.

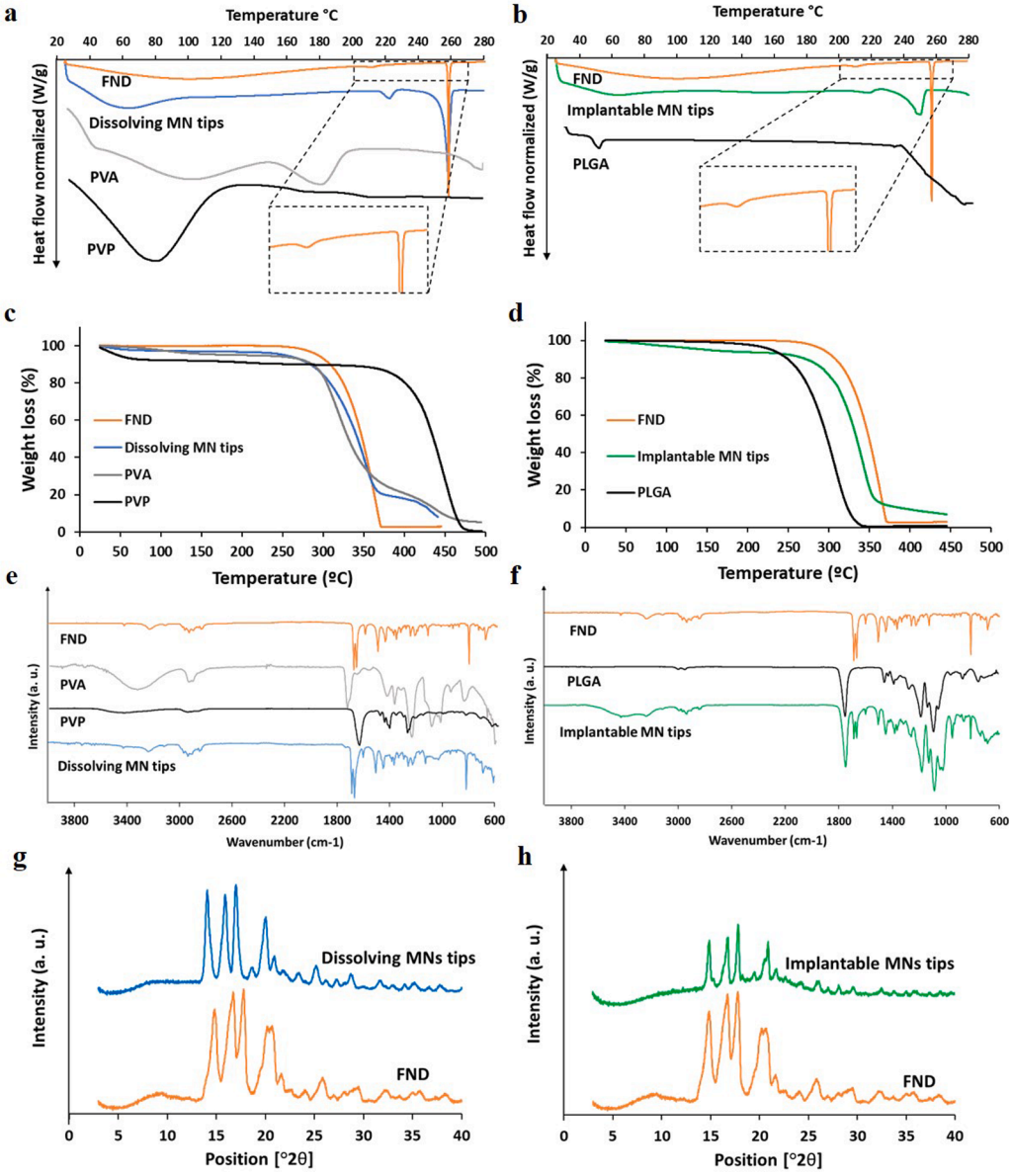

Fig. 6. Physicochemical characterisation of FND and FND loaded dissolving and implantable MAPs. **a**- Differential scanning calorimetry (DSC) of FND, dissolving MN tips, PVP and PVA. **b**- Differential scanning calorimetry (DSC) of FND, implantable MN tips and PLGA. **c**- Thermogravimetric analysis (TGA) of FND, dissolving MN tips, PVP and PVA. **d**- Thermogravimetric analysis (TGA) of FND, implantable MN tips and PLGA. **e**- Fourier transformed infrared spectra of FND, PVP, PVA, and dissolving MN tips. **f**- Fourier transformed infrared spectra of FND, PLGA and implantable MN tips. **g**- Powder X-ray diffraction of FND and dissolving MN tips. **h**- Powder X-ray diffraction of FND and implantable MN tips.

analyses shown in Fig. 6**c and d** revealed that the coarse drug, dissolving and implantable MAPs, and their correspondent excipients were stable even at high temperatures, with decomposition of both dissolving and implantable MN tips starting at approximately 260 °C. Moreover, they also shown negligible weight loss in the temperature range of 25–100 °C, indicating that the samples did not contain significant amounts of water.

FTIR study was used to further evaluate the compatibility of FND with the excipients in the various formulations. The FTIR spectra of FND, dissolving MNs, PVP and PVA are shown in Fig. 6**e**, whereas the spectra of FND, the implantable MNs and PLGA are shown in Fig. 6**f**. In the FND spectrum, the peaks found at 1365 cm^{-1} and 1383 cm^{-1} were attributed to *tert*-butyl group. Other peaks observed at 1666 cm^{-1} and 1688 cm^{-1}, were attributed to the two amide groups of C = O stretching band. Finally, the presence of peaks at 3430 cm^{-1} and 3243 cm^{-1} were due to the amide group of N–H stretching band. In both formulations, all the characteristics peaks of FND were also observed, indicating that FND did not interact with other excipients used in the formulations.

The PXRD patterns of FND alone and loaded into dissolving and implantable MAPs can be observed in Fig. 6**g** and **h,** respectively. In both samples, the characteristic peaks of the coarse drug (i.e., at 14, 16, 17 and 20 °2θ) were also observed, thus confirming that the drug kept its crystalline characteristics in the final formulations. However, in the case of the implantable MN tips, the intensity of the peaks was reduced. This, together with the less intense melting peak observed in the DSC experiment, indicate a degree of amorphization of the drug within the PLGA matrix. Furthermore, PXRD experiments allowed to confirm that the polymorphic form I of FND was present in the coarse drug and in both MAPs, and no polymorphic transformation took place during the formulation process. Crucially, the X-ray diffraction pattern of form I is clearly distinguishable from that of the form II as described in the literature (da Silva et al., 2015). All together, these results demonstrate that the formulation of FND into dissolving MNs using the combination of PVA and PVP, as well as implantable MNs using PLGA, allowed FND to keep its crystalline characteristics, with no polymorphic transformations of FND during the manufacture of the MAPs, and no interactions observed between drug and excipients.

3.4. *Particle size analysis*

The particle size distribution of coarse FND and FND dispersed from the dissolving MAPs can be observed in Fig. 7. Coarse FND presented a monomodal distribution, with mean diameters [D4,3] and [D3,2] of

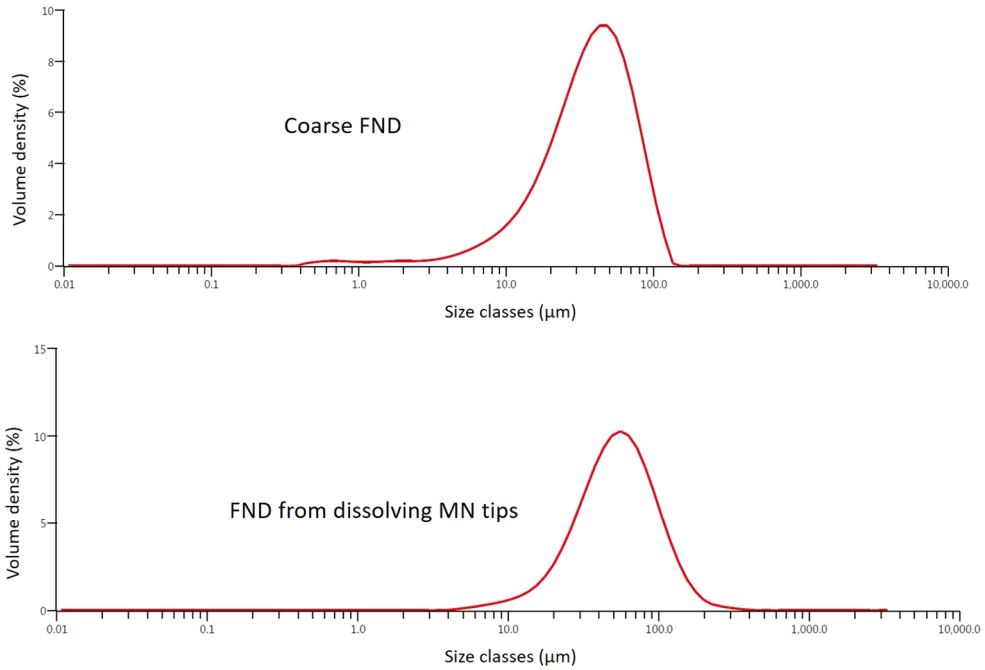

Fig. 7. Particle size distribution of coarse FND and FND redispersed from dissolving MAPs obtained by lase diffraction.

41.6 μm and 16.8 μm, respectively (D_{10}: 12.1 μm, D_{50}: 37.7 μm, D_{90}: 77.2 μm). Similarly, the redispersion of FND from the dissolving MN produced a monomodal distribution with mean diameters [D4,3] and [D3,2] of 61.1 μm and 40.4 μm, respectively (D_{10}: 22.6 μm, D_{50}: 52.6 μm, D_{90}: 109.0 μm). Implantable MN tips were not analysed by laser diffraction since the drug is entrapped in the PLGA matrix, which impedes its redispersion as discrete particles and their detection by the laser of the instrument.

3.5. Drug content and distribution in the MAPs

The drug content in dissolving and implantable MAPs, and the drug distribution between the baseplate and MN tips, is shown in Fig. 8. Dissolving MAPs were able to load 2697.86 ± 402.29 μg of FND, with 2256.95 ± 112.82 μg accumulated in the MN tips and 343.30 ± 29.63 μg remaining in the baseplate. In the case of implantable PLGA MAPs, the total amount of drug loaded was 1715.21 ± 273.61 μg, of which 1475.83 ± 237.59 μg were in the MN tips and 249.76 ± 29.28 μg in the baseplate. The presence of FND in the baseplate is explained by the back-migration of the drug from the MNs to the baseplate aqueous blend during the manufacture process; this phenomenon is commonly observed in water soluble drugs, a phenomenon less commonly observed with poorly soluble drugs. FND is slightly soluble in water (<2 mg/ml), which in combination with the increased wettability provided by PVP in the baseplate (Maniruzzaman et al., 2013), increased the chances of drug back-migration. However, it is important to highlight that only 12.72% and 14.56% of the FND was located in the baseplate for dissolving and implantable MAPs, respectively.

3.6. In vitro drug release

In vitro release profiles of FND from the coarse drug, compared to the dissolving and implantable MN tips were obtained over 14 days. As observed in Fig. 9, dissolving MAPs presented the highest dissolution rate in comparison to the coarse drug and the implantable formulation, reaching a maximum drug by day 7. After 48 h, when a plateau in the dissolution rate was observed, 76.43 ± 19.22% of drug was released from dissolving MAPs, whereas for the coarse drug and implantable MAPs, the amounts of FND dissolved were 61.43 ± 9.53% and 35.51 ± 0.93% respectively. At this time point, no significant differences were observed between the dissolving formulation and the coarse drug ($p > 0.05$ in both cases). On the contrary, the differences between the implantable and the other two formulations were found to be statistically significant ($p < 0.05$). Until day 11, the same trend in dissolution

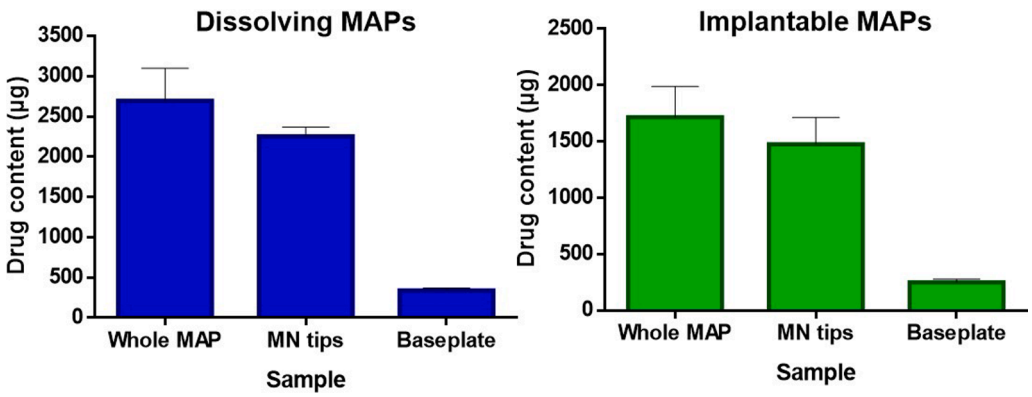

Fig. 8. Drug content and distribution in dissolving and implantable MAPs.

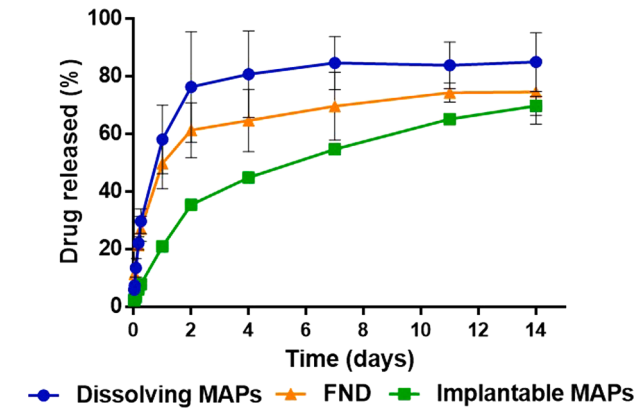

Fig. 9. *In vitro* drug release profiles of FND from pure FND, dissolving MAPs and implantable MAPs using a dialysis membrane (12,000–14,000 MWCO) experimental set up. Results expressed as means ± SD, n = 3.

profiles was observed, with similar differences among the groups maintained throughout this period. Finally, after 14 days, the amounts of drug released from dissolving MAPs, coarse drug and implantable MAPs were 85.09 ± 10.17%, 74.74 ± 11.18%, and 69.90 ± 3.28% respectively, with no statistical differences among the three samples analysed ($p > 0.05$). The use of dialysis membranes for the study of the release behaviour of different drugs has been widely used as a predictor of the *in vitro* and *in vivo* performance of long-acting MAPs (Permana et al., 2020, 2019b; Tekko et al., 2020; Volpe-Zanutto et al., 2021). Crucially, the drug release rate determined using this model has been found to be markedly faster than that observed in subsequent *ex vivo* and *in vivo* release experiments, with this phenomenon attributed to the difference in the volume available for dissolution, naturally lower in the viable layers of the skin (Permana et al., 2020; Rojekar et al., 2021; Yao et al., 2017). In spite of that, it is crucial to ensure the maintenance of sink conditions, which permits the evaluation of the drug release system independently from solvent volume and consequently from saturation effects, both factors that can influence drug dissolution (Siepmann and Siepmann, 2013). According to the results observed here, both the dissolving and implantable formulations hold promise with respect to the long-acting release of FND, since demonstrating utility for drug delivery over 7 and 14 days, respectively.

3.7. Skin deposition in studies in Franz cells

Skin experiments in Franz cells revealed that both formulations were able to localise considerable amounts of the drug in the skin as well as to release FND to the receptor compartment of the Franz cells. As shown in Fig. 10**a**, dissolving and implantable MAPs deposited 629.00 ± 214.54 μg and 1861.64 ± 383.30 μg of FND in the skin, respectively, with significant difference between the groups ($p < 0.05$). Moreover, dissolving and implantable MAPs were able to deliver 90.43 ± 6.20 μg and 22.08 ± 6.15 μg of FND to the receptor compartment, respectively at 24 h. When considering the amount of drug deposited in the skin, to the best of our knowledge, no other system could deliver higher FND payloads than those observed in this work. For example, Rao *et al.* (Rao et al., 2008), prepared vesicular ethosomal carriers that was only managed to deliver around 25 μg/cm^2 of FND to the skin. Another report by Kim *et al.* described the use powder-carrying MAPs that deposited approximately 44.70 ± 8.14 μg/cm^2 of FND in the skin (S. Kim et al., 2019). Adjusted by area (the MN area of the patches described here is 0.5 cm^2), the implantable and dissolving MAPs deposited amounts of FND that were 50- and 148-fold superior to the ethosomal formulation, respectively, and 28- and 84-fold higher than the powder carrying MAPs, respectively. The main reason for this phenomenon is the high MN density of the MAPs prepared in this work, which allowed greater loading capacity of FND, leading to a noticeable increase in the drug deposited within the skin. Similar results were previously observed when a similar MAP archetype was used to deliver the hydrophobic drugs cabotegravir (Tekko et al., 2019), itraconazole (Permana et al., 2020) and etravirine (Rojekar et al., 2021). Once MAPs are inserted *in vitro*, the fluids of the dermis dissolve the drug, which then freely diffuses into deeper skin layers, eventually reaching the solvent in the receptor compartment. *In vivo*, this translates into the absorption of the drug to the plasmatic circulation, with consequent systemic effects (Cole et al., 2019; Liu et al.,

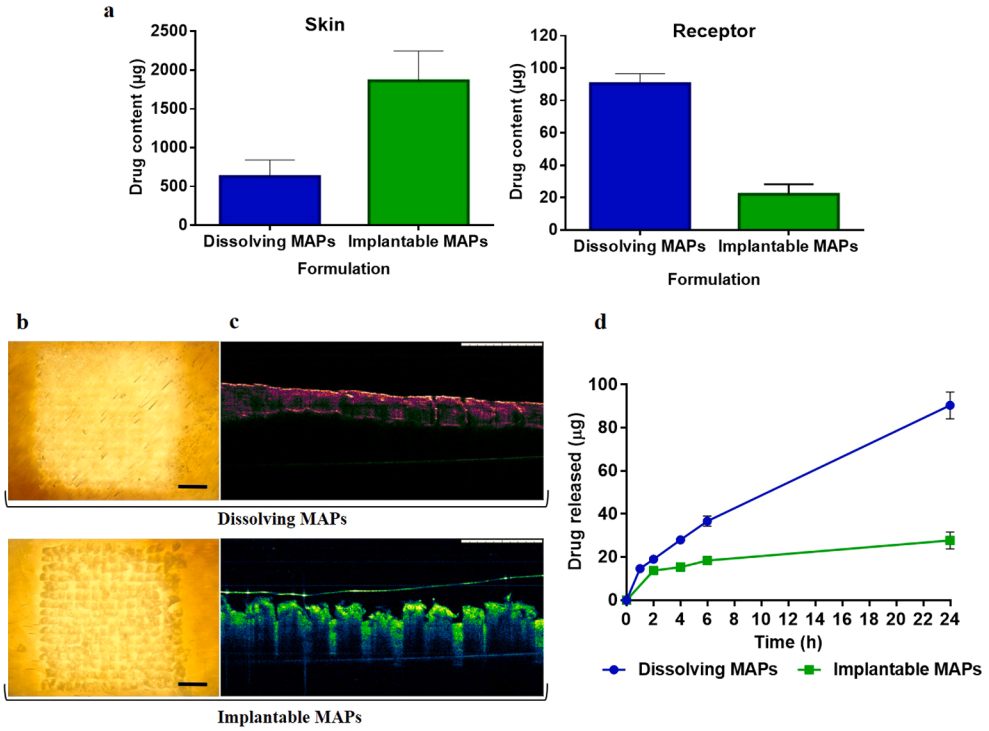

Fig. 10. Skin experiments of FND MAPs. a- FND deposition in skin, receptor compartment after application of dissolving and implantable MAPs to excised neonatal full-thickness porcine skin, results expressed as means ± SD, n = 4. b- optical microscopy images of the skin area where dissolving and implantable MAPs were applied after the endpoint of the study. Scale bars = 1 mm c- optical coherence tomography of the skin area where dissolving and implantable MAPs were applied after the endpoint of the study. Scale bars = 1 mm. d-transdermal drug permeation of for dissolving and implantable MAPs, results expressed as means ± SD, n = 4.

2021; Volpe-Zanutto et al., 2021). Giffen *et al.* recently reported the use of dissolvable MAPs for the systemic delivery of the drug dutasteride (Giffen et al., 2020), another 5α-reductase inhibitor used for the treatment of prostatic hyperplasia, achieving a sustained release of the drug in rats (Giffen et al., 2020). Moreover, the *in silico* modelling of this data predicted that the formulation could be administered to humans every two weeks (Giffen et al., 2020). In our work, dissolving and implantable MAPs demonstrated their capacity to deliver FND to the receptor compartments of the Franz cells, which highlights the potential use of these novel formulations for the treatment of benign prostate hyperplasia, where FND requires systemic distribution to reach the androgen-dependent tissues of the prostate (Gormley et al., 1992).

Fig. 10**b** shows photomicrographs of the MAPs application areas after the 24 h skin deposition experiment, where dissolving MAPs created a pattern of indentations in the skin that follows the MAP geometry, revealed by the use of light from the stereo-microscope illuminated from the underside of the skin sample. These skin markings are produced by the insertion of the MNs and posterior dissolution of the excipients and the drug. Conversely, for implantable MAPs, the area of application was covered by the PLGA MN tips, with their square appearance attributed to the MN pedestals. In order to confirm this observation, OCT images were obtained for both formulations. As shown in Fig. 10**c**, the skin sample treated with dissolving MAPs presented a number of marks on the outer surface, which were approximately 100 μm in depth. The insertion of MAPs creates these pores in the skin, which tend to close after application due to the inherent flexibility of the epidermis (Brogden et al., 2012). OCT analysis of the skin area confirmed MN insertion, as the triangular MN tips were easily detectable. This provided further evidence supporting the fact that implantable PLGA MAPs produce MNs capable of piercing the skin, creating micro-implants with the potential for prolonged drug delivery. In order to evaluate the capacity of the novel dissolving and implantable FND MAPs to deliver the drug over a sustained period, transdermal permeation experiments were carried out in Franz cells. As shown in Fig. 10**d**, there was a marked difference between the transdermal release profiles of both FND MAPs. On the one hand, dissolving MAPs were able to deliver a maximum of 90.43 ± 6.20 μg by the experimental endpoint (24 h). Implantable MAPs, on the other hand, delivered only 27.80 ± 3.94 μg of FND after 24 h, with this value proving statistically different from that of the dissolving MAPs ($p < 0.05$). Unsurprisingly, the release rate of FND from the PLGA micro-implants was low due to the capacity of this polymer to degrade slowly in the body. Our findings are in agreement with the results observed in other reports, where PLGA was able to produce MNs suitable for skin penetration, releasing active compounds over prolonged periods, both *in vitro* and *in vivo* (He et al., 2020; Li et al., 2019a, 2019b).

When MAPs are applied in the skin, slowly-dissolving drug depots are left in the dermis, from where the drug diffuses and is absorbed by the blood microvasculature housed within the dermis. Whereas the transdermal drug release from dissolving MAPs is governed by a slow dissolution of the 61.1 μm-drug particles, FND release from implantable formulations is largely controlled by the presence of PLGA, which forms a matrix from where the drug must dissolve and diffuse. The use of PLGA for the formulation of MAPs holds promise in terms of long-acting release (He et al., 2020; Li et al., 2019a, 2019b; Peng et al., 2021). To date, a relatively low number of reports have described the use of PLGA MAPs to release drugs for weeks and months, however, the biodegradation of PLGA in the skin is still not fully understood. In a recent study, Peng *et al* delivered amphotericin B using PLGA MN tips and demonstrated that the length of the tips was reduced to 50% in size after incubation in PBS for 21 days (Peng et al., 2021). However, further experiments on long-term skin application and biodegradation of the polymer are still required to fully understand the mechanisms of drug release from such matrices.

Importantly, drug absorption via this route ultimately results in body wide distribution due to the systemic circulation (Paredes et al., 2020b; Vora et al., 2021). In the implantable MAPs developed here, PLGA played a key role in controlling the release of FND, whereas, in the dissolving formulation, the release of the drug was controlled by the physicochemical properties of FND (i.e., particle size: 61.1 μm, aqueous solubility: 1.98 μg/ml; log P: 3.03). According to the data observed in this work, the application of these MAPs to the skin has the potential to release the drug for several days. Dissolving MAPs, deposited 629 μg of FND in the skin, from which only 90 μg were delivered in 24 h, which in theory means that this formulation has the potential to release the active for 7 days. Using a similar analysis, the implantable MAPs could release the active compound for up to 67 days. This, together with the 14-days release experiments, provides robust evidence that both dissolving and implantable MAPs can release their drug cargo over prolonged periods. However, further pharmacokinetic studies in animal models are required to shed light on the time periods in which these MAPs would maintain therapeutic plasma levels of FND, which in humans is reported to be 0.012 μg/l (Ko and Jusko, 1995; Steiner, 1996).

4. Conclusions

Novel bi-layered dissolving and implantable FND MAPs were produced using a casting technique. Both formulations presented a high drug loading capacity and sufficient mechanical resistance to penetrate the skin. The physicochemical characterisation evidenced that the crystallinity of the drug was maintained during the formulation process, with no observed interactions between the drug and the excipients. *In vitro* release experiments using sink conditions evidenced that implantable MAPs delivered the drug over 14 days, whereas and *ex vivo* studies demonstrated that the novel MAPs were capable of slowly delivering the active drug to the skin, but also transdermally. Together, *in vitro* and *ex vivo* release experiments suggest that the formulations developed here can efficiently deliver FND to the skin during prolonged periods, therefore constituting a potential user-friendly option for patients suffering from BPH and androgenic alopecia. However, *in vivo* complementary studies are necessary to fully understand the pharmacokinetics of these FND MAPs.

CRediT authorship contribution statement

Alejandro J. Paredes: Conceptualization, Methodology, Investigation, Formal analysis, Writing – original draft, Writing – review & editing. **Fabiana Volpe-Zanutto:** Methodology, Investigation. **Andi Dian Permana:** Investigation. **Aidan J. Murphy:** Investigation. **Camila J. Picco:** Methodology, Investigation. **Lalitkumar K. Vora:** Investigation. **Jonathan A. Coulter:** Conceptualization, Writing – review & editing. **Ryan F. Donnelly:** Conceptualization, Supervision, Funding acquisition, Writing – original draft, Writing – review & editing.

Declaration of Competing Interest

The authors declare that they have no known competing financial interests or personal relationships that could have appeared to influence the work reported in this paper.

Appendix A. Supplementary data

Supplementary data to this article can be found online at https://doi.org/10.1016/j.ijpharm.2021.120885.

References

Abdelghany, S., Tekko, I.A., Vora, L., Larrañeta, E., Permana, A.D., Donnelly, R.F., 2019. Nanosuspension-based dissolving microneedle arrays for intradermal delivery of curcumin. Pharmaceutics 11, 308. https://doi.org/10.3390/pharmaceutics11070308.

Ahmed, T.A., 2016. Preparation of finasteride capsules-loaded drug nanoparticles: Formulation, optimization, in vitro, and pharmacokinetic evaluation. Int. J. Nanomedicine 11, 515–527. https://doi.org/10.2147/IJN.S98080.

Brogden, N.K., Milewski, M., Ghosh, P., Hardi, L., Crofford, L.J., Stinchcomb, A.L., 2012. Diclofenac delays micropore closure following microneedle treatment in human subjects. J. Control. Release 163, 220–229. https://doi.org/10.1016/j.jconrel.2012.08.015.

Chen, Z., He, J., Qi, J., Zhu, Q., Wu, W., Lu, Y., 2020. Long-acting microneedles : a progress report of the state-of-the-art techniques. Drug Discov. Today 25, 1462–1468. https://doi.org/10.1016/j.drudis.2020.05.006.

Chiu, Y.-W., Teitelbaum, I., Misra, M., de Leon, E.M., Adzize, T., Mehrotra, R., 2009. Pill Burden, Adherence, Hyperphosphatemia, and Quality of Life in Maintenance Dialysis Patients. Clin. J. Am. Soc. Nephrol. 4, 1089 LP – 1096. https://doi.org/10.2215/CJN.00290109.

Claborn, K.R., Meier, E., Miller, M.B., Leffingwell, T.R., 2015. A systematic review of treatment fatigue among HIV-infected patients prescribed antiretroviral therapy. Psychol. Health Med. 20, 255–265. https://doi.org/10.1080/13548506.2014.945601.

Cole, G., Ali, A.A., McErlean, E., Mulholland, E.J., Short, A., McCrudden, C.M., McCaffrey, J., Robson, T., Kett, V.L., Coulter, J.A., Dunne, N.J., Donnelly, R.F., McCarthy, H.O., 2019. DNA vaccination via RALA nanoparticles in a microneedle delivery system induces a potent immune response against the endogenous prostate cancer stem cell antigen. Acta Biomater. 96, 480–490. https://doi.org/10.1016/j.actbio.2019.07.003.

Courtenay, A.J., McAlister, E., McCrudden, M.T.C., Vora, L., Steiner, L., Levin, G., Levy-Nissenbaum, E., Shterman, N., Kearney, M.-C., McCarthy, H.O., Donnelly, R.F., 2020. Hydrogel-forming microneedle arrays as a therapeutic option for transdermal esketamine delivery. J. Control. Release 322, 177–186 https://doi.org/https://doi.org/10.1016/j.jconrel.2020.03.026.

D'Amico, A.V., Roehrborn, C.G., 2007. Effect of 1 mg/day finasteride on concentrations of serum prostate-specific antigen in men with androgenic alopecia: a randomised controlled trial. Lancet Oncol. 8, 21–25. https://doi.org/10.1016/S1470-2045(06)70981-0.

da Silva, L.M., Montanari, C.M., Santos, O.M.M., Cazedey, E.C.L., Ângelo, M.L., de Araújo, M.B., 2015. Quality evaluation of the Finasteride polymorphic forms I and II in capsules. J. Pharm. Biomed. Anal. 105, 24–31. https://doi.org/10.1016/j.jpba.2014.11.045.

Donnelly, R.F., Garland, M.J., Morrow, D.I.J., Migalska, K., Raghu, T., Singh, R., Majithiya, R., Woolfson, A.D., 2010. Optical coherence tomography is a valuable tool in the study of the effects of microneedle geometry on skin penetration characteristics and in-skin dissolution. J. Control. Release 147, 333–341.

Donnelly, R.F., Larrañeta, E., 2018. Microarray patches: potentially useful delivery systems for long-acting nanosuspensions. Drug Discov. Today 23, 1026–1033. https://doi.org/10.1016/j.drudis.2017.10.013.

Giffen, P.S., Bhuiya, R., Brackenborough, K., Hobbs, M.J., Qian, L., Burke, M.D., 2020. Controlled Delivery of Dutasteride Using Dissolvable Microarrays: Initial Formulation and In Vivo Evaluation. J. Pharm. Sci. 109, 1303–1311. https://doi.org/10.1016/j.xphs.2019.11.012.

Goodman, P.J., Tangen, C.M., Darke, A.K., Scott Lucia, M., Ford, L.G., Minasian, L.M., Parnes, H.L., LeBlanc, M.L., Thompson, I.M., 2019. Long-Term effects of finasteride on prostate cancer mortality. N. Engl. J. Med. 380, 393–394. https://doi.org/10.1056/NEJMc1809961.

Gormley, G.J., Stoner, E., Bruskewitz, R.C., Imperato-Mcginley, J., Walsh, P.C., Mcconnell, J.D., Andriole, G.L., Geller, J., Bracken, B.R., Tenover, J.S., Vaughan, E.D., Pappas, F., Taylor, A., Binkowitz, B., Ng, J., 1992. The Effect of Finasteride in Men with Benign Prostatic Hyperplasia. N. Engl. J. Med. 327, 1185–1191.

He, M., Yang, G., Zhao, X., Zhang, S., Gao, Y., 2020. Intradermal Implantable PLGA Microneedles for Etonogestrel Sustained Release. J. Pharm. Sci. 109, 1958–1966. https://doi.org/10.1016/j.xphs.2020.02.009.

Kim, J.H., Na, J., Bak, D.H., Lee, B.C., Lee, E., Choi, M.J., Ryu, C.H., Lee, S., Mun, S.K., Park, B.C., Kim, B.J., Lee, H.S., 2019a. Development of finasteride polymer microspheres for systemic application in androgenic alopecia. Int. J. Mol. Med. 43, 2409–2419. https://doi.org/10.3892/ijmm.2019.4149.

Kim, S., Eum, J., Yang, H., Jung, H., 2019b. Transdermal finasteride delivery via powder-carrying microneedles with a diffusion enhancer to treat androgenetic alopecia. J. Control. Release 316, 1–11. https://doi.org/10.1016/j.jconrel.2019.11.002.

Ko, H.C., Jusko, W.J., 1995. Pharmacodynamic modeling of finasteride, a 5 alpha-reductase inhibitor. Pharmacotherapy 15, 509–511.

Kumar, R., Singh, B., Bakshi, G., Katare, O.P., 2007. Development of liposomal systems of finasteride for topical applications: design, characterization, and in vitro evaluation. Pharm. Dev. Technol. 12, 591–601. https://doi.org/10.1080/10837450701481181.

Larrañeta, E., Lutton, R.E.M., Woolfson, A.D., Donnelly, R.F., 2016. Microneedle arrays as transdermal and intradermal drug delivery systems: Materials science, manufacture and commercial development. Mater. Sci. Eng. R Reports 104, 1–32 https://doi.org/https://doi.org/10.1016/j.mser.2016.03.001.

Larrañeta, E., Moore, J., Vicente-Pérez, E.M., González-Vázquez, P., Lutton, R., Woolfson, A.D., Donnelly, R.F., 2014. A proposed model membrane and test method for microneedle insertion studies. Int. J. Pharm. 472, 65–73. https://doi.org/10.1016/j.ijpharm.2014.05.042.

Lee, J.W., Park, J.H., Prausnitz, M.R., 2008. Dissolving microneedles for transdermal drug delivery. Biomaterials 29, 2113–2124. https://doi.org/10.1016/j.biomaterials.2007.12.048.

Li, W., Tang, J., Terry, R.N., Li, S., Brunie, A., Callahan, R.L., Noel, R.K., Rodríguez, C.A., Schwendeman, S.P., Prausnitz, M.R., 2019a. Long-acting reversible contraception by effervescent microneedle patch. Sci. Adv. 5, eaaw814. https://doi.org/10.1126/sciadv.aaw8145.

Li, W., Terry, R.N., Tang, J., Feng, M.R., Schwendeman, S.P., Prausnitz, M.R., 2019b. Rapidly separable microneedle patch for the sustained release of a contraceptive. Nat. Biomed. Eng. 3, 220–229. https://doi.org/10.1038/s41551-018-0337-4.

Liu, T., Jiang, G., Song, G., Sun, Y., Zhang, X., Zeng, Z., 2021. Fabrication of rapidly separable microneedles for transdermal delivery of metformin on diabetic rats. J. Pharm, Sci https://doi.org/https://doi.org/10.1016/j.xphs.2021.04.009.

Maniruzzaman, M., Rana, M.M., Boateng, J.S., Mitchell, J.C., Douroumis, D., 2013. Dissolution enhancement of poorly water-soluble APIs processed by hot-melt extrusion using hydrophilic polymers. Drug Dev. Ind. Pharm. 39, 218–227. https://doi.org/10.3109/03639045.2012.670642.

Mc Crudden, M.T.C., Larrañeta, E., Clark, A., Jarrahian, C., Rein-Weston, A., Lachau-Durand, S., Niemeijer, N., Williams, P., Haeck, C., McCarthy, H.O., Zehrung, D., Donnelly, R.F., 2018. Design, formulation and evaluation of novel dissolving microarray patches containing a long-acting rilpivirine nanosuspension. J. Control. Release 28, 119–129. https://doi.org/10.1016/j.jconrel.2018.11.002.

Mir, M., Ahmed, N., Permana, A.D., Rodgers, A.M., Donnelly, R.F., Rehman, A.U., 2019. Enhancement in site-specific delivery of carvacrol against methicillin resistant staphylococcus aureus induced skin infections using enzyme responsive nanoparticles: A proof of concept study. Pharmaceutics 11, 606.

NHS, 2020. Finasteride [WWW Document]. Medicines. URL https://www.nhs.uk/medicines/finasteride/ (accessed 5.4.21).

Paredes, A.J., Camacho, N.M., Schofs, L., Dib, A., Zarazaga, M. del P., Litterio, N., Allemandi, D.A., Sánchez Bruni, S., Lanusse, C., Palma, S.D., 2020a. Ricobendazole nanocrystals obtained by media milling and spray drying: Pharmacokinetic comparison with the micronized form of the drug. Int. J. Pharm. 585, 119501. https://doi.org/https://doi.org/10.1016/j.ijpharm.2020.119501.

Paredes, A.J., Mckenna, P.E., Ramöller, I.K., Naser, Y.A., Volpe-Zanutto, F., Li, M., Abbate, M.T.A., Zhao, L., Zhang, C., Abu-ershaid, J.M., Dai, X., Donnelly, R.F., 2020b. Microarray Patches: Poking a Hole in the Challenges Faced When Delivering Poorly Soluble Drugs. Adv. Funct. Mater. 2005792, 1–27. https://doi.org/10.1002/adfm.202005792.

Paredes, A.J., Ramöller, I.K., McKenna, P.E., Abbate, M.T.A., Volpe-Zanutto, F., Vora, L.K., Kilbourne-Brook, M., Jarrahian, C., Moffatt, K., Zhang, C., Tekko, I.A., Donnelly, R.F., 2021. Microarray patches: Breaking down the barriers to contraceptive care and HIV prevention for women across the globe. Adv. Drug Deliv. Rev. 173, 331–348 https://doi.org/https://doi.org/10.1016/j.addr.2021.04.002.

Peng, K., Vora, L.K., Domínguez-Robles, J., Naser, Y.A., Li, M., Larrañeta, E., Donnelly, R.F., 2021. Hydrogel-forming microneedles for rapid and efficient skin deposition of controlled release tip-implants. Mater. Sci. Eng., C 127, 112226 https://doi.org/https://doi.org/10.1016/j.msec.2021.112226.

Permana, A.D., Anjani, Q.K., Sartini, Utomo, E., Volpe-Zanutto, F., Paredes, A.J., Evary, Y.M., Mardikasari, S.A., Pratama, M.R., Tuany, I.N., Donnelly, R.F., 2021. Selective delivery of silver nanoparticles for improved treatment of biofilm skin infection using bacteria-responsive microparticles loaded into dissolving microneedles. Mater. Sci. Eng. C 120, 111786. https://doi.org/https://doi.org/10.1016/j.msec.2020.111786.

Permana, A.D., Paredes, A.J., Volpe-Zanutto, F., Anjani, Q.K., Utomo, E., Donnelly, R.F., 2020. Dissolving microneedle-mediated dermal delivery of itraconazole nanocrystals for improved treatment of cutaneous candidiasis. Eur. J. Pharm. Biopharm. 154, 50–61. https://doi.org/10.1016/j.ejpb.2020.06.025.

Permana, A.D., Tekko, I.A., McCrudden, M.T.C., Anjani, Q.K., Ramadon, D., McCarthy, H.O., Donnelly, R.F., 2019. Solid lipid nanoparticle-based dissolving microneedles: A promising intradermal lymph targeting drug delivery system with potential for enhanced treatment of lymphatic filariasis. J. Control. Release 316, 34–52. https://doi.org/10.1016/j.jconrel.2019.10.004.

Pervaiz, F., Saleem, M., Ashames, A., Rehmani, S., Qaiser, R., Noreen, S., Murtaza, G., 2020. Development and ex-vivo skin permeation studies of finasteride–poly(lactic acid-co-glycolic acid) and minoxidil–chitosan nanoparticulate systems. J. Bioact. Compat. Polym. 35, 77–91. https://doi.org/10.1177/0883911520913906.

Rao, Y., Zheng, F., Zhang, X., Gao, J., Liang, W., 2008. In Vitro Percutaneous Permeation and Skin Accumulation of Finasteride Using Vesicular Ethosomal Carriers. AAPS PharmSciTech 9, 860–865. https://doi.org/10.1208/s12249-008-9124-y.

Rojekar, S., Vora, L.K., Tekko, I.A., Volpe-Zanutto, F., McCarthy, H.O., Vavia, P.R., Donnelly, R.F., 2021. Etravirine-loaded dissolving microneedle arrays for long-acting delivery. Eur. J. Pharm, Biopharm https://doi.org/https://doi.org/10.1016/j.ejpb.2021.04.024.

Roque, L.V., Dias, I.S., Cruz, N., Rebelo, A., Roberto, A., Rijo, P., Reis, C.P., 2017. Design of Finasteride-Loaded Nanoparticles for Potential Treatment of Alopecia. Skin Pharmacol. Physiol. 30, 197–204. https://doi.org/10.1159/000475473.

Siepmann, J., Siepmann, F., 2013. Mathematical modeling of drug dissolution. Int. J. Pharm. 453, 12–24 https://doi.org/https://doi.org/10.1016/j.ijpharm.2013.04.044.

Simonazzi, A., Cid, A.G., Paredes, A.J., Schofs, L., Gonzo, E.E., Palma, S.D., Bermúdez, J.M., 2018. Development and in vitro evaluation of solid dispersions as strategy to improve albendazole biopharmaceutical behavior. Ther. Deliv. 9, 623–638. https://doi.org/10.4155/tde-2018-0037.

Soleymani, S.M., Salimi, A., 2019. Enhancement of Dermal Delivery of Finasteride Using Microemulsion Systems. Adv. Pharm. Bull. 9, 584–592 https://doi.org/10.15171/apb.2019.067.

Steiner, J.F., 1996. Clinical pharmacokinetics and pharmacodynamics of finasteride. Clin. Pharmacokinet. https://doi.org/10.2165/00003088-199630010-00002.

Summerfield, A., Meurens, F., Ricklin, M.E., 2015. The immunology of the porcine skin and its value as a model for human skin. Mol. Immunol. 66, 14–21. https://doi.org/10.1016/j.molimm.2014.10.023.

Tabbakhian, M., Tavakoli, N., Jaafari, M.R., Daneshamouz, S., 2006. Enhancement of follicular delivery of finasteride by liposomes and niosomes 1. In vitro permeation

and in vivo deposition studies using hamster flank and ear models. Int. J. Pharm. 323, 1–10. https://doi.org/10.1016/j.ijpharm.2006.05.041.

Tekko, I., Vora, L., McCrudden, M., Jarrahian, C., Rein-Weston, A., Zehrung, D., Giffen, P., McCarthy, H., Donnelly, R., 2019. 2019 Control. Release Soc. Annu. Meet. Expo, in: Novel Dissolving Bilayer Microarray Patches as a Minimally Invasive, Efficient Intradermal Delivery System for a Longacting Cabotegravir Nanosuspension. Valencia.

Tekko, I.A., Pemana, D., Vora, L., Hatahet, T., Mccarthy, H.O., Donnelly, R.F., 2020. Localised and sustained intradermal delivery of methotrexate using nanocrystal-loaded microneedle arrays : Potential for enhanced treatment of psoriasis. Eur. J. Pharm. Sci. 152, 105469 https://doi.org/10.1016/j.ejps.2020.105469.

Thompson, I.M., Goodman, P.J., Tangen, C.M., Lucia, M.S., Miller, G.J., Ford, L.G., Lieber, M.M., Cespedes, R.D., Atkins, J.N., Lippman, S.M., Carlin, S.M., Ryan, A., Szczepanek, C.M., Crowley, J.J., Coltman, C.A., 2003. The Influence of Finasteride on the Development of Prostate Cancer. N. Engl. J. Med. 349, 215–224. https://doi.org/10.1056/NEJMoa60.

Van Der Maaden, K., Jiskoot, W., Bouwstra, J., 2012. Microneedle technologies for (trans)dermal drug and vaccine delivery. J. Control. Release 161, 645–655.

Volpe-Zanutto, F., Ferreira, L., Permana, A.D., Kirkby, M., Paredes, A.J., Vora, L., Bonfanti, A., Charlie-Silva, I., Raposo, C., Figueiredo, M.C., Souza, I.M.O., Brisibe, A., Costa, F.D., Donnelly, R.F., Foglio, M.A., 2021. Artemether and lumefantrine dissolving microneedle patches with improved pharmacokinetic performance and antimalarial efficacy in mice infected with Plasmodium yoelii. Release Article in Press, J. Control.

Vora, L.K., Moffatt, K., Tekko, I.A., Paredes, A.J., Volpe-Zanutto, F., Mishra, D., Peng, K., Raj Singh Thakur, R., Donnelly, R.F., 2021. Microneedle array systems for long-acting drug delivery. Eur. J. Pharm. Biopharm. 159, 44–76. https://doi.org/10.1016/j.ejpb.2020.12.006.

Wawrzycka, I., Stępniak, K., Matyjaszczyk, S., Kozioł, A.E., Tadeusz, L., Abboud, K.A., 1999. Structural characterization of polymorphs and molecular complexes of finasteride. J. Mol. Struct. 474, 157–166. https://doi.org/10.1016/S0022-2860(98)00569-9.

Yang, J., Liu, X., Fu, Y., Song, Y., 2019. Recent advances of microneedles for biomedical applications: drug delivery and beyond. Acta Pharm. Sin. B 9, 469–483 https://doi.org/https://doi.org/10.1016/j.apsb.2019.03.007.

Yao, G., Quan, G., Lin, S., Peng, T., Wang, Q., Ran, H., Chen, H., Zhang, Q., Wang, L., Pan, X., Wu, C., 2017. Novel dissolving microneedles for enhanced transdermal delivery of levonorgestrel: In vitro and in vivo characterization. Int. J. Pharm. 534, 378–386. https://doi.org/10.1016/j.ijpharm.2017.10.035.